Numerical investigation on effects of steel I-section beams on the blast resistance of a stiffened steel tank under blast loading

Indexed by:
Web of Science Group

Yunhao Li[a,b*], Song Lin[a,b*], Zhixiang Xing[a,b], Qi Zhang[a,c], Yunying Pi[b], Juncheng Jiang[a,b]

[a] Engineering Laboratory of Battery Safety and Accident Control of Petroleum and Chemical Industry, Changzhou University, Changzhou 213164, China
[b] School of Safety Science and Engineering, Changzhou University, No. 21 Gehu mid Rd., Changzhou 213164, China
[c] College of Safety and Environmental Engineering, Shandong University of Science and Technology, Qingdao 266590, China

Highlights

- Structural reliability of a steel tank with horizontal stiffeners under blast loading.

- Horizontal stiffening ring enhanced the overall structural integrity of a steel tank.

- Larger beam dimensions contribute to increased bending and shear stiffness.

Abstract

The hazardous chemical storage tank faces a vital explosion risk, making reliability a critical concern. This study investigates the horizontal stiffening ring as an effective anti-blast measure to enhance the reliability of steel tanks under explosive conditions. Through numerical examination based on CONWEP model, we assessed the impact of vertical spacing between adjacent horizontal stiffening rings and their dimensions on the tank's blast resistance and overall structural integrity. The results suggest that a marked improvement in the tank's reliability and blast resistance with the addition of stiffening rings as horizontal stiffeners. The deformation shapes of the stiffened steel tank were less pronounced, and the radial displacements were smaller compared to an unstiffened steel tank. Additionally, the addition of horizontal stiffening rings enhanced the overall stiffness and stability of the steel tank. Furthermore, larger beam dimensions contribute to increased bending and shear stiffness, resulting in smaller deformations and better blast resistance of the steel tank.

Keywords

storage tank, structural reliability, blast loading, structural integrity, failure mechanisms, finite element simulation.

1. Introduction

Since the mid-1950s, oil has been regarded as the main fuel, playing a key role in social development and the global economy [1]. However, its status as a hazardous chemical underscores the critical importance of reliability in oil storage infrastructure. The catastrophic consequences of oil tank failures highlight the urgent need for enhanced structural reliability to safeguard human health, the environment, and economic stability. These failures, often resulting in extreme cascading effects, demonstrate the interconnected nature of tank reliability within oil storage facilities [2-4]. A stark illustration of this reliability challenge occurred on August 6, 2022, at an oil depot in Matanzas Province, Cuba. A lightning strike on a single tank containing 25,000 m³ of oil triggered a catastrophic chain of events, exposing the vulnerability of the entire storage system. The initial tank's structural failure led to a fire that spread to adjacent tanks, resulting in multiple explosions and compromising the integrity of surrounding storage units (Fig. 1). By August 8, a third tank had exploded, further threatening

(*) Corresponding author.
E-mail addresses: Y. Li (ORCID: 0000-0003-3158-8129) liyunhao@cczu.edu.cn, S. Lin (ORCID: 0000-0002-5248-1120) LS@cczu.edu.cn, Z. Xing xingzhixiang@cczu.edu.cn, Q. Zhang zhangqi2021@sdust.edu.cn, Y. Pi 2034329300@qq.com, J. Jiang jiangjc@cczu.edu.cn,

nearby structures and emphasizing the critical need for improved reliability across the entire tank farm. This incident's severe human toll - 1 death, 128 injuries, and 14 missing firefighters [5] - underscores the dire consequences of insufficient reliability in hazardous material storage systems and the imperative for more robust, failure-resistant designs [6].

Recognizing the critical need for enhanced structural reliability in hazardous material storage, numerous researchers have focused on investigating the impact of blast events on thin-walled structures or assess the reliability of thin-walled structures under blast events [6]. Duong et al. investigated the deformation mode of an empty tank fall into gas explosion [7]. Clubley studied the structure response of aluminum cylindrical tanks under long-duration shock wave [8]. They also examined the impact of fluid levels on the structure response of cylindrical, aluminum-made tanks [9]. Zhang et al. quantitatively analyzed the explosion consequences of a gas tank using TNT-equivalent explosion model [10]. Wang and Zhou numerically investigated the structural behaviors of a steel tank filled with water exposed to shock wave [11]. Zhang et al. conducted a numerical study to examine how a spherical steel tank filled with liquid responds to blast loading. [12]. Hu and Zhao numerically investigated the internal gas explosion characteristic in fixed-roof vertical tanks [13]. Pickerd et al. examined structure response and failure mechanism of steel containers exposed to internal explosions [14]. Abo-Elkhier et al. investigated the basic failure reasons of a toluene storage tank due to boiled liquid expanded vapor explosions [15]. Hu et al. numerically investigated the dynamic response of a large vertical tank impacted by blast fragments [16]. Li et al. examined the interaction of the shock wave with pressurized container under BLEVE [17, 18]. Chen et al. numerically researched the structural behavior and deformation mode of water-filled steel tanks met with double blast loadings [19]. Rokhy et al. numerically analyzed the structural behavior of aluminum shells exposed to gas explosion [20]. Studziński et al. established a 3-stage FE approach for investigating a sandwich panel subjected to blast wave [21]. Jiang et al. proposed a numerical method to model the uncertainty propagation of domino effect related to blast events [22].

For the anti-blast design of thin-walled structures, Su and Zhai numerically investigated the anti-blast performance of anti-blast wall on a reticulated shell [23]. Zheng et al. experimentally examined the impact of the stiffener on the structural behavior of a steel plate under interior explosion [24]. Bornstein et al. explored the anti-blast performance of the geometry of a water-filled tank [25]. Jiang et al. researched the anti-blast performance of the polyurea coating on vertical oil tanks [26]. Wu et al. numerically analyzed the effect of interior pressure and the inner diameter on the blast resistance of the steel pipeline [27]. Jiang et al. examined the anti-blast impact of polyurea coating on the steel oil tank under long duration blast loading [28]. Gan et al. explored the anti-explosion effect of the stiffened plate exposed to explosion from different shapes of cuboid explosives [29]. Wang et al. numerically researched the impact of the cross-section and spacing of anti-blast bands on the dynamic response of vertical oil tanks [30]. Zhao et al. analyzed the preventive effect of the bund system on the tank failure [31].

According to the literature review, while numerous studies have investigated the response of thin-walled structures to blast events, there's a lack of research specifically addressing reliability improvement strategies. Moreover, the majority of studies concentrate on structural response and failure modes, with fewer investigations from the perspective of improving overall system reliability. According to Chinese National Standard GB 50341 [32] or API Standard 650 [33], one or several stiffening rings could be installed at appropriate positions on the vertical cylinder of the large steel storage tank to improve the tank's resistance to external pressure. Despite recommendations in standards for installing stiffening rings on large steel storage tanks, there is limited research on their effect on the anti-blast performance of these structures.

In this research, a numerical model was constructed using the finite element analysis code Abaqus. The effectiveness and accuracy of the numerical model were verified against the experimental results in Ref. [26]. Then, the anti-blast effect of the horizontal stiffening ring on the steel tank was studied. Finally, the study analyzed the effects of the vertical spacing between adjacent horizontal stiffening rings and the dimensions of these rings on the steel tank's blast resistance.

This study aims to address the anti-blast performance of horizontal stiffening rings on large steel storage tanks, an area that has been understudied despite being recommended in industry standards. By systematically analyzing the effects of

stiffening ring spacing and dimensions, the research provides valuable insights into optimizing structural designs for blast resistance. The study contributes to improving the overall safety and reliability of hazardous material storage infrastructure.

Fig. 1. A fire and explosion accident of an oil depot in the port of Matanzas Province, Cuba.

2. Numerical modelling

2.1. Geometry

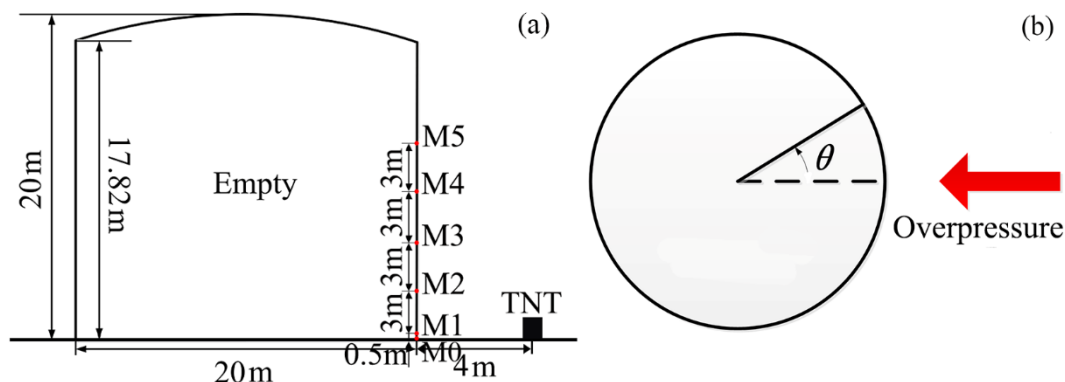A fixed-roof steel tank with dimensions of 20 m (diameter) × 20
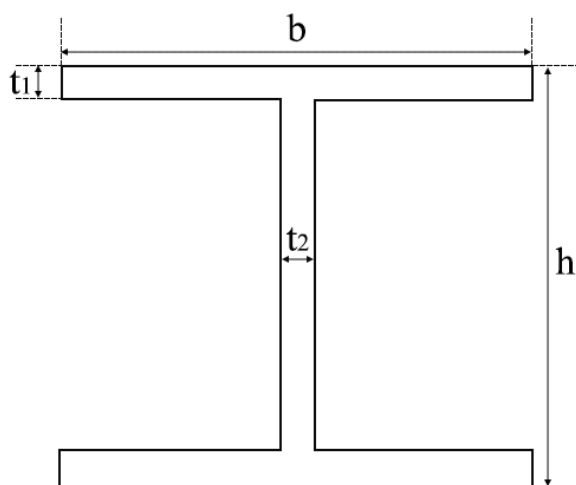
m (height), and a holding capacity of 5000 m^3, was selected for this study. And the thickness of the steel shell was 12 mm. The schematic diagram of the steel tank is illustrated in Fig. 2. The steel tank was empty in all cases to simulate the worst scenario. The distance between the steel tank and the TNT explosive was 4 m. And the mass of the TNT explosive was 200 kg. Six monitoring points, M0, M1, M2, M3, M4, and M5, were arranged along the meridian at $\theta=0°$ to measure the overpressure and displacement evolution process (Fig. 2 (a)). M0 was set at the welding joint between the bottom plate and cylindrical shell. The vertical distance between M0 and M1 was 0.5 m. The vertical distance between M1, M2, M3, M4 and M5 was 3 m.

To improve the stiffness of the steel tank, steel I-section beams were installed inside it. Dimensions of types 14, 16, 18, 20, and 22 according to the Chinese standard were selected for this research. Fig. 3 presents the schematic diagram of the steel I-section beam. Besides, Table 1 lists five steel I-section beams with different dimensions.

Fig. 2. Schematic diagram of the steel tank.

Fig. 3. Schematic diagram of the steel I-section beam.

Table.1. Dimensions of five steel I-section beams.

Type	Height (h), mm	width (b), mm	Flange thickness (t$_1$), mm	Web thickness (t$_2$), mm
14	140	80	9.1	5.5
16	160	88	9.9	6.0
18	180	94	10.7	6.5
20	200	100	11.4	7.0
22	220	110	12.3	7.5

2.2. Finite element model

Fig. 4 depicts the view cut of the finite element model of the stiffened steel tank. The finite element model of the steel I-section beam utilized the element type B31. B31 is a 2-node linear beam in space. B31 is a type of Timoshenko beam that

takes account of transverse shear deformation. The quadrilateral finite-membrane-strain element S4R was used for the tank walls and bottom plates. S4R is a 4-node, quadrilateral, stress/displacement shell element with reduced integration and a large-strain formulation. The tie constraint, which equalizes the translational and rotational motion between a pair of surfaces, was used to connect the cylindrical shell to the steel I-section beam. The bottom of the steel tank was also fixed to the ground.

The Johnson-Cook plasticity model was used for the steel tank and steel I-section beam. Johnson-Cook plasticity model was defined as Eq. (1) [34].

$$\bar{\sigma}=\left[A+B\left(\bar{\varepsilon}^{pl}\right)^n\right]\left[1+C\ln\left(\frac{\dot{\varepsilon}^{pl}}{\dot{\varepsilon}_0}\right)\right](1-T^m) \tag{1}$$

where $\bar{\sigma}$ is the yield stress at nonzero strain rate, $\dot{\varepsilon}_0$ is the reference strain rate, $\bar{\varepsilon}^{pl}$ is the equivalent plastic strain rate, A, B, C, m, n are material constants. As the maximum strain experienced by the steel tank was less than 0.2 during the blast experiments, the resulting temperature change within the tank was negligible [26]. Consequently, the temperature-dependent parameters T and m were not considered in this study. Table 2 lists Johnson-Cook parameters of the low carbon steel.
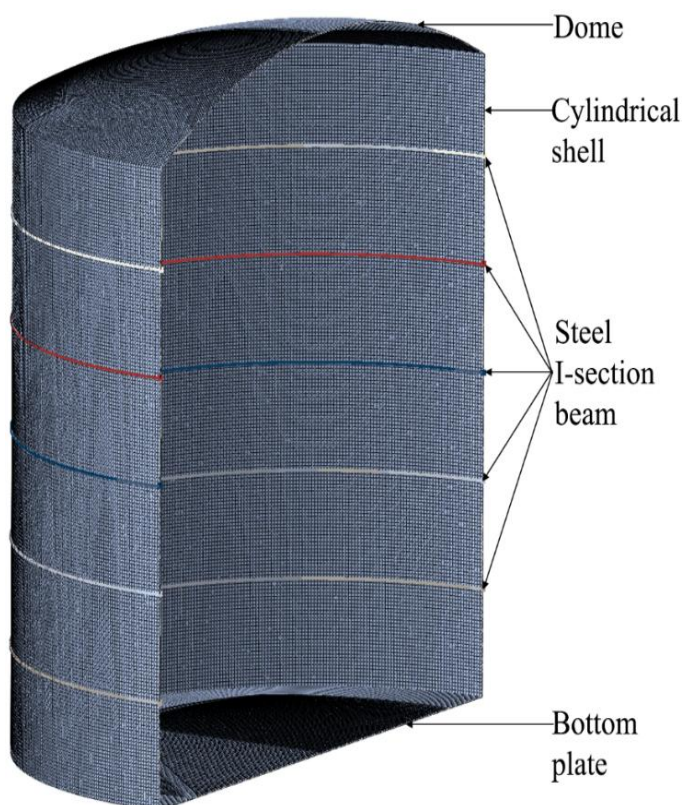

Fig. 4. Finite element model of the stiffened steel tank (View cut along X plane).

Table.2 Johnson-Cook parameters of the low carbon steel.

A, MPa	B, MPa	C	n	Reference strain rate, s^{-1}
210	372	0.04938	0.4521	0.0006

2.3. CONWEP (Conventional Weapons Effects Program) model

The CONWEP model is a widely used empirical model that predicts the effects of a conventional explosion, such as a bomb, on its surroundings. The model uses the scaled distance which is a dimensionless quantity that relates the distance from the explosion to the yield of the explosive. CONWEP assumes an exponential decay of the pressure with time as described by Eq. (2)-(4) [35]:

$$P_i(t)=P_{i0}\left[1-\frac{t_s-t_a}{t_d}\right]\exp\left[\frac{-a(t_s-t_a)}{t_d}\right] \tag{2}$$

$$P_r(t)=P_{r0}\left[1-\frac{t_s-t_a}{t_d}\right]\exp\left[\frac{-b(t_s-t_a)}{t_d}\right] \tag{3}$$

$$P(t)=P_r(t)\cos^2\theta+P_i(t)(1+\cos^2\theta-2\cos\theta) \tag{4}$$

Where P is the total pressure on the structure, P_{i0} is the peak pressure of the incident wave, P_{r0} is the peak pressure of the reflected wave, θ is the incident angle, t_d is the duration of positive pressure, t_a is the arrival time of the shock wave, t_s is the relative time of the system, a and b are the attenuation factors of the pressure of the incident and reflected waves, respectively.

Since the TNT was placed on the ground, the resulting blast was a surface burst with a hemispherical shape. To model this type of explosion, Ullah et al. [36] suggested using a globular TNT explosive with an increased TNT equivalent, achieved by multiplying an amplification factor λ due to reflection. λ was determined by the material of the base surface and ranged from 0.85 to 0.9 for concrete ground [37]. In this study, λ was set to 0.9 to account for the concrete ground surface.

2.4. Mesh sensitivity analysis

Three mesh sizes—0.2 m (with 89,742 elements), 0.1 m (with 190,598 elements), and 0.05 m (with 458,522 elements), were applied in the mesh sensitivity analysis. Overpressure and radial displacement versus time at the monitoring point M1 for different mesh sizes are displayed in Fig. 5. Considering computational efficiency and accuracy, a mesh size of 0.1 m was selected for the subsequent numerical simulations.
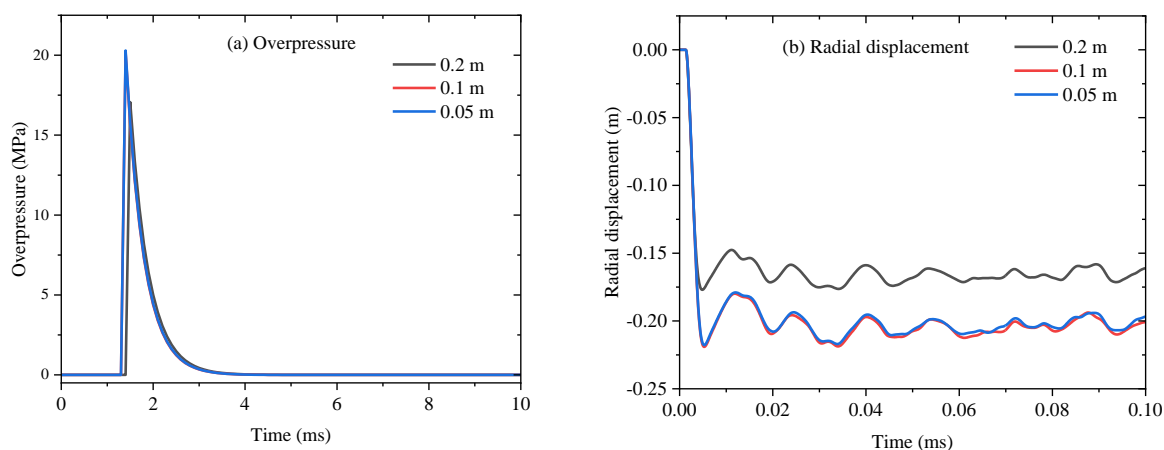
Fig. 5. Overpressure and radial displacement vs. time for different mesh sizes.

3. Validation studies

A field test of a steel tank subjected to TNT explosion carried out by Jiang et al. [26], was used to verified the reliability and accuracy of the finite element model. Fig. 6 shows the schematic diagram of the experimental setup. The steel tank was welded by 1-mm low carbon steel plates. The cylindrical TNT charge was 2 kg. The standoff distance between the TNT explosive and steel tank was 3.2 m. A displacement sensor was fixed on the cylindrical shell of the steel tank to record the displacement evolution. In the finite element model, the steel tank was modeled using shell elements. The overpressure was predicted using the CONWEP model. The global mesh size was 15 mm. Table 3 shows the comparison of the setup of the finite element model between this paper and reference [26].

Fig. 7 illustrates the comparison of the radial displacement between the numerical simulation and experimental test. The evolution of the finite element analysis result showed good agreement with the experimental result. The radial displacement predicted by the finite element analysis was very close to that from the experimental result. Fig. 8 shows the comparison of the deformation shape between the finite element simulation and experimental test. The deformation zone and the shape of the plastic hinge lines from the finite element analysis were similar to those observed in the experimental results. Thus, the finite element model used in this study can predict the dynamic response behavior of the steel tank when subjected to blast loading.
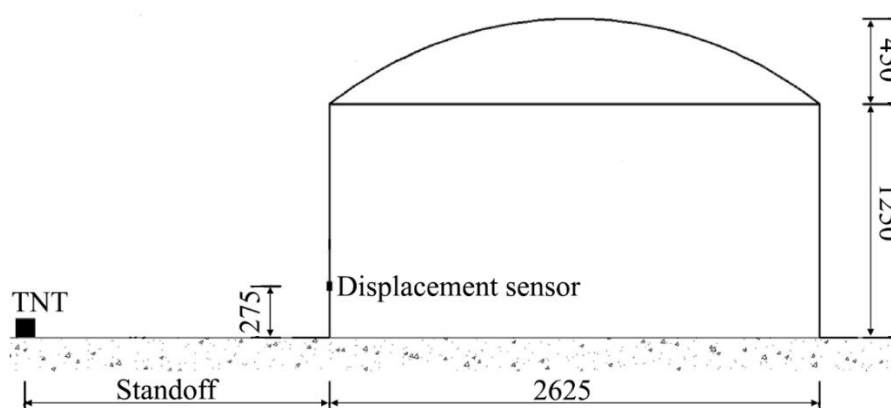

Fig.6. Schematic diagram of the experimental setup by Jiang et al. [26]. (unit: mm).

Table. 3 Comparison of the setup of the finite element model between this paper and reference [26].

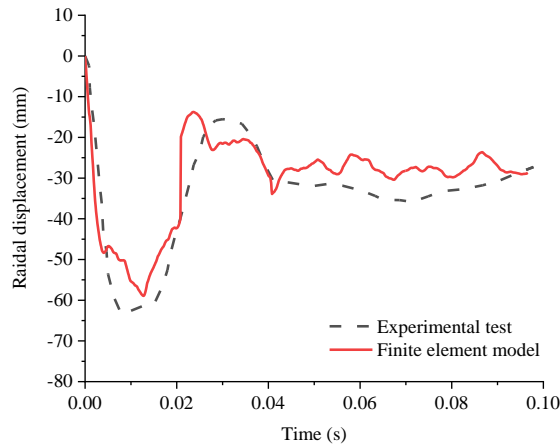| Article	Software	Numerical model for blast loading	Element type of the tank	Material model	Mesh size
Reference	LS-DYNA	CONWEP	Shell, S4R	Johnson-Cook	13 mm
This paper	Abaqus	CONWEP	Shell, S4R	Johnson-Cook	15 mm

Fig. 7. Comparison of the radial displacement between the FE simulation and experimental tests.

(a) Experimental test (b) Finite element simulation

Fig. 8. Comparison of the deformation shape between the FE simulation and second test.

4. Results and discussion

4.1. Dynamic response of the stiffened steel tank

Fig. 9 shows the overpressure evolution curves at five monitoring points. Fig. 10 depicts the temporal and spatial distribution of overpressure on the cylindrical shell of a stiffened steel tank. The shock wave first encountered the bottom of the cylindrical shell. Meanwhile, the overpressure on the cylindrical shell also reached at 19.7 MPa (M0). Then, the shock wave propagated along the cylindrical shell. And the overpressure reached its peak at 20 MPa (M1). The contour of the overpressure distribution resembled an arch caused by a hemispherical TNT explosion. And the maximum overpressure was located at the top of the arch. Moreover, the maximum overpressure decreased sharply with the time increasing.

Fig. 11 illustrates the deformation shapes of the stiffened steel tank and steel I-section beams at different times. When the shock wave reached the cylindrical shell of the stiffened steel tank, the bottom of the shell and the steel I-section beam

deformed. Then, as the shock wave transmitted upward along the cylindrical shell, the deformation zone of the shell and the steel I-section beam further expanded. Besides, the peak deformation zone moved up as the explosion expanded.
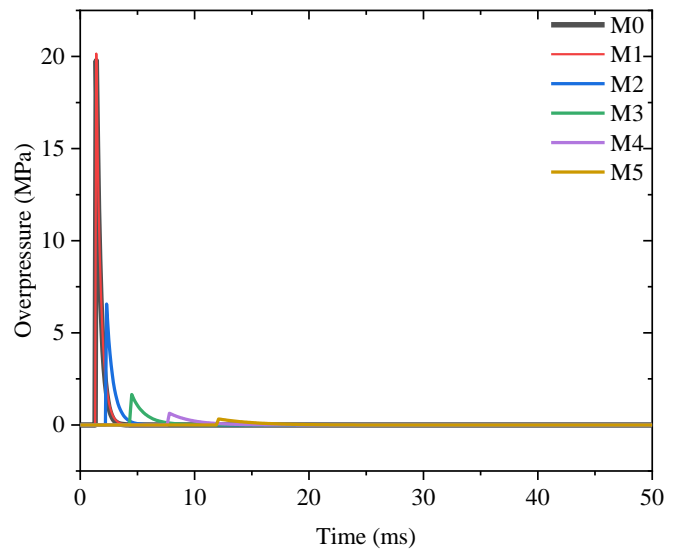

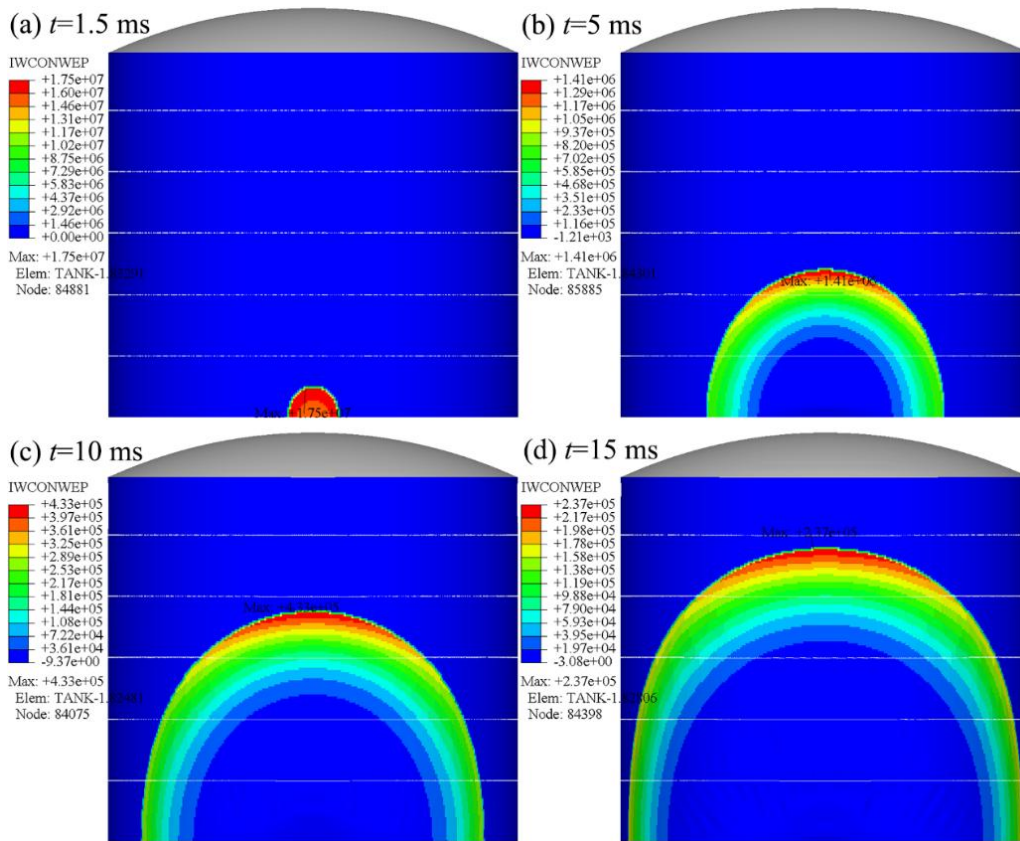Fig. 9. Overpressure vs. time in different monitoring points.

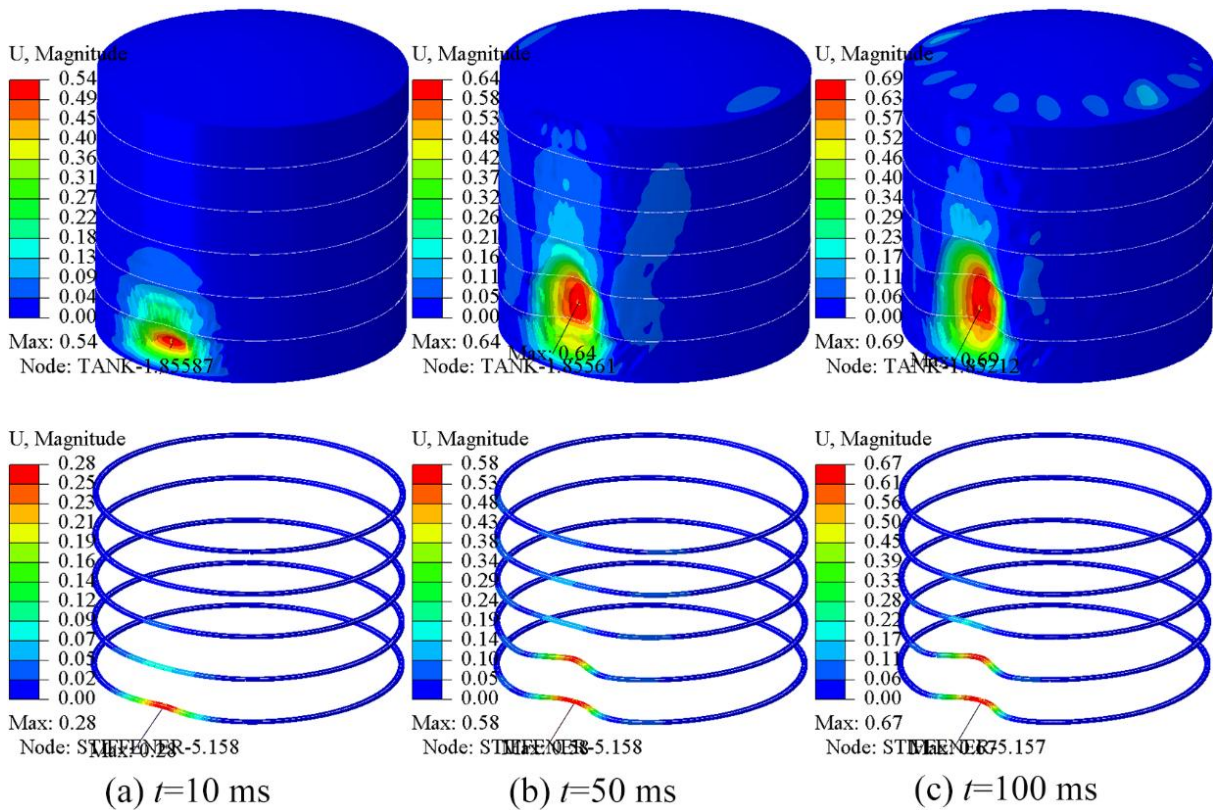Fig. 10. Temporal and spatial overpressure distributions on the cylindrical shell of a stiffened steel tank.

Fig. 11. Deformation shapes vs. time of the stiffened steel tank and steel I-section beams.

4.2. Comparison between the unstiffened and stiffened steel tanks

Fig. 12 illustrates the radial displacement comparison at monitoring points between stiffened and unstiffened steel tanks. The onset of dynamic response of the stiffened steel tank at each monitoring point was basically the same as that of the unstiffened steel tank. The radial displacement at monitoring point M0 and M1 for the stiffened steel tank was nearly equal to that of the unstiffened steel tank. The radial displacements at monitoring points M3 and M4 for the stiffened steel tank were significantly smaller than those of the unstiffened steel tank. Besides, the radial displacement at the welding joint between the bottom plate and cylindrical shell was less than that at the depression zone due to the constriction of the bottom plate.

Fig. 13 shows the comparison of the deformation shape between stiffened and unstiffened steel tanks at $t = 100$ ms. Fig. 14 depicts the comparison of radial displacement distributions along the meridian $\theta=0°$ and the circumference with the largest radial displacement at $t = 100$ ms. Entire steel tanks were basically deformed, including domes. The deformation of the stiffened steel tank was less severe than that of the unstiffened

steel tank. Besides, circumferential and meridional depression ranges of the unstiffened steel tank were larger than those of the stiffened steel tank. The height of the depression zone in the meridional direction was approximately 9 m, and the range in the circumferential direction was approximately 40° for the stiffened steel tank. The height of the depression zone in the meridional direction was approximately 15 m. The range in the circumferential direction was approximately 50° for the unstiffened steel tank.

The reason is that the addition of steel I-section beam to the cylindrical shell of the tank significantly enhances its overall stiffness and stability under blast loading. These beams serve as additional load-carrying members, redistributing stresses concentrations in the regions of the shell that are not stiffened (Fig. 15). They provide increased resistance to bending and hoop stress, mitigating excessive deformation and potential failure modes. Furthermore, the unstiffened tank absorbed and dissipated a larger portion of the blast energy through deformation of the shell. Consequently, the enhanced stiffness and stability imparted by the beam improve the tank's resistance to deformation and failure, ensuring safer operation under blast loading.
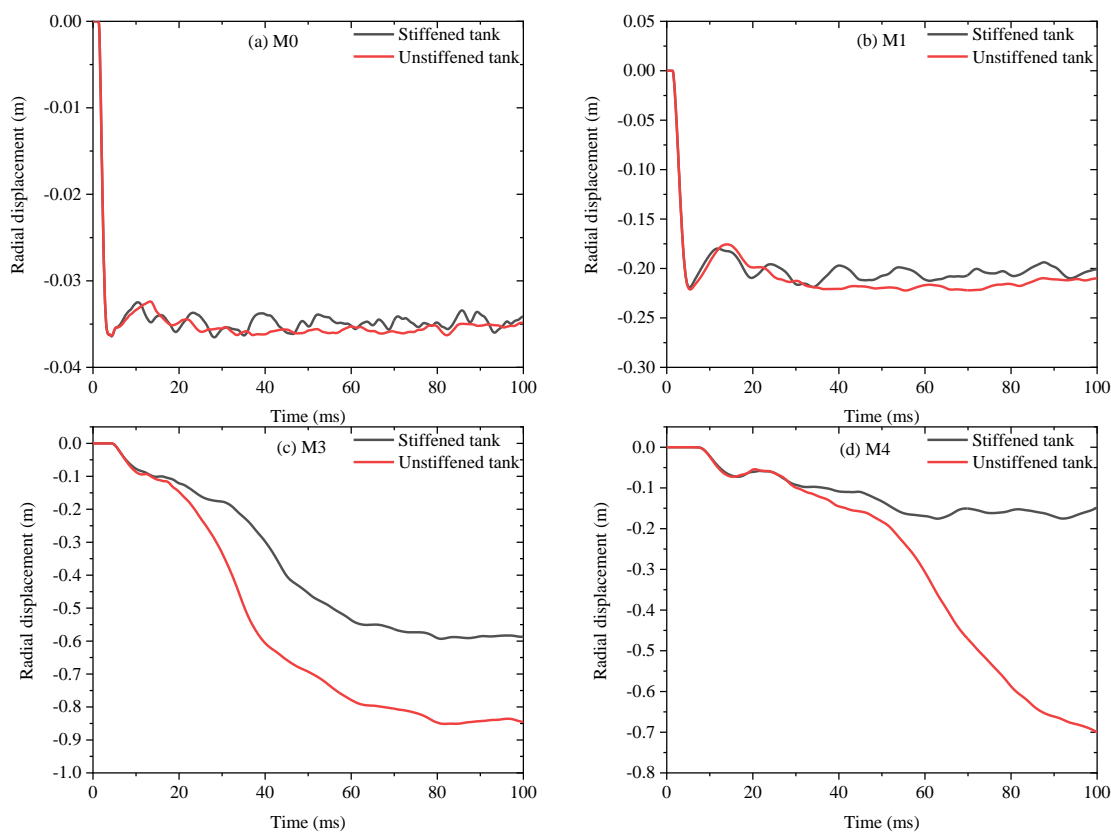

Fig. 12. Comparison of the radial displacement of monitoring points between stiffened and unstiffened steel tanks.
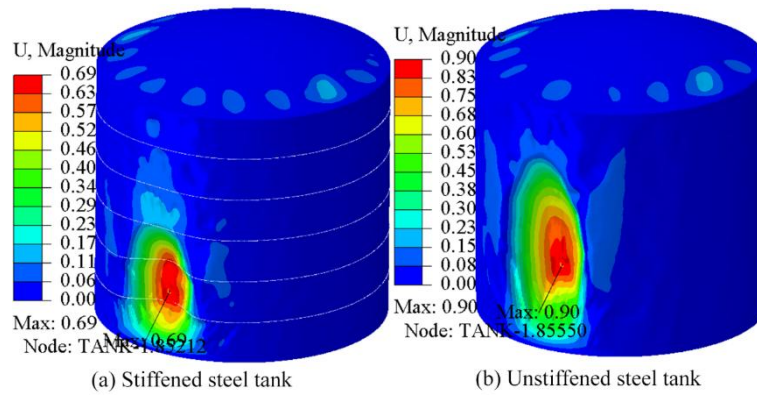
(a) Stiffened steel tank

(b) Unstiffened steel tank

Fig. 13. Comparison of the deformation shape between stiffened and unstiffened steel tanks at t=100 ms.

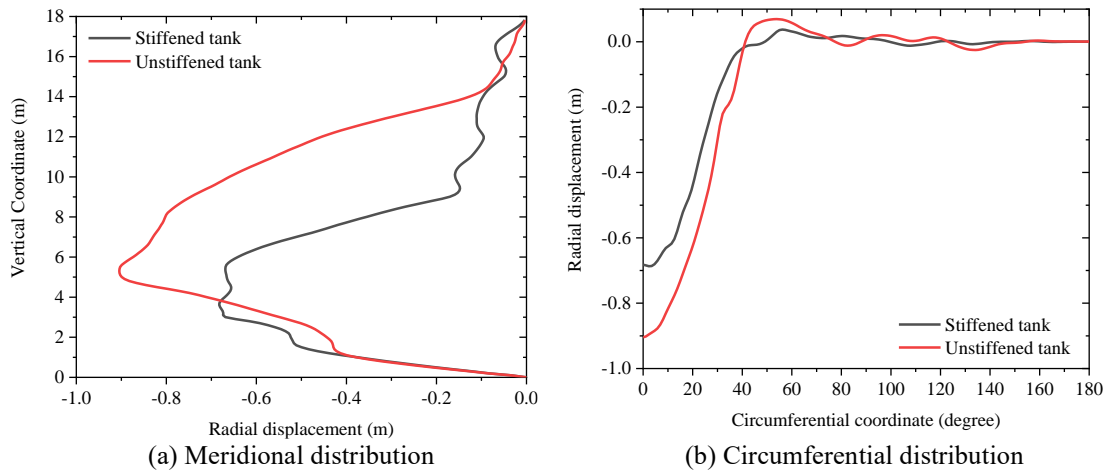
(a) Meridional distribution

(b) Circumferential distribution

Fig. 14. Comparison of radial displacement distributions along the meridian $\theta = 0°$ (a) and the circumference with largest radial displacement (b) between stiffened and unstiffened steel tanks $t = 100$ ms.
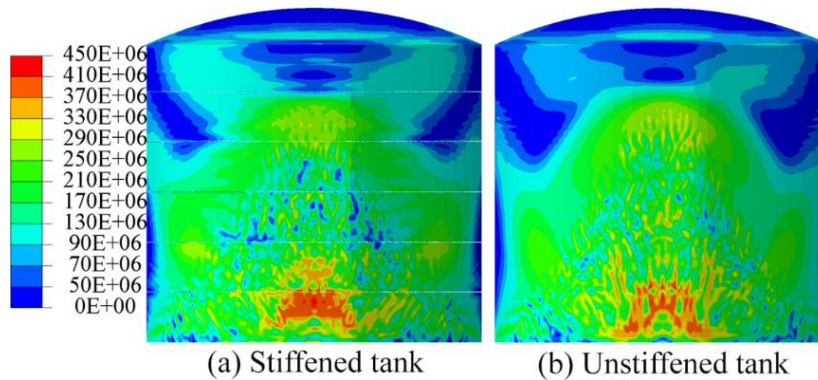

(a) Stiffened tank

(b) Unstiffened tank

Fig. 15. Comparison of the Von Mises stress between stiffened and unstiffened steel tanks at t=20 ms.

4.3. Effect of the vertical spacing between adjacent two steel I-section beams

The effect of the vertical spacing between adjacent steel I-section beams on the dynamic response of the stiffened steel tank was investigated in this section. Vertical spacings of 2, 3, 4, 5, and 6 m, corresponding to 8, 5, 4, 3, and 2 steel I-section beams respectively, were selected.

Fig. 16 shows deformation shapes of stiffened steel tanks for different vertical spacings. Fig. 17 illustrates radial displacement distributions along the meridian $\theta = 0°$ and the circumference with the largest radial displacement. The deformation and maximum radial displacement increased with the vertical spacing. The maximum deformation zone moved upwards with the vertical spacing increasing. Besides, the cylindrical shell depressed from the bottom to the dome in the vertical direction along the meridian $\theta = 0°$.

The reason is that closer vertical spacing of the beams

generally led to an increase in the stiffness of the stiffened steel tank. With a reduced distance between the beams, the cylindrical shell of the tank was better supported and reinforced at multiple locations, resulting in improved load distribution and reduced bending deformations. Conversely, larger vertical spacing between the beams led to increased unsupported spans of the tank shell, allowing for greater deformations and potentially higher stress concentrations. Additionally, closely spaced beams provided more effective resistance to buckling and instability of the tank shell under compressive loading. Moreover, the shell absorbed more energy, while the steel I-section beam absorbed less, especially as the amount of the steel I-section beam decreased. Thus, the stiffness of the stiffened steel tank decreased as the vertical spacing increased. The deformation, depression, and maximum radial displacement were more serious as the vertical spacing increased.
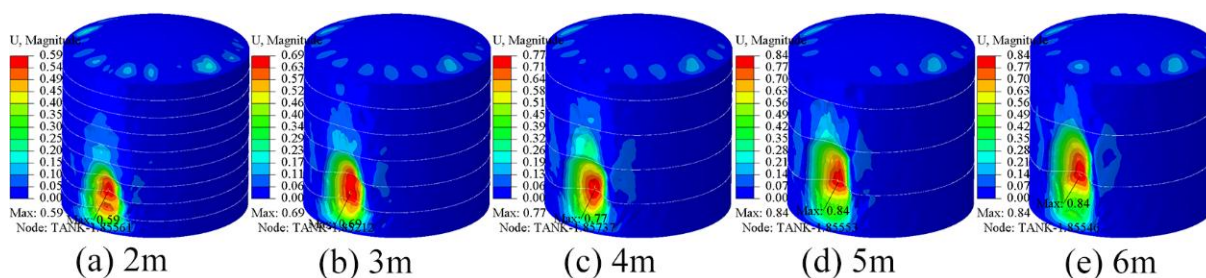

Fig. 16. Deformation shapes of stiffened steel tanks for different vertical spacings at $t = 100$ ms.
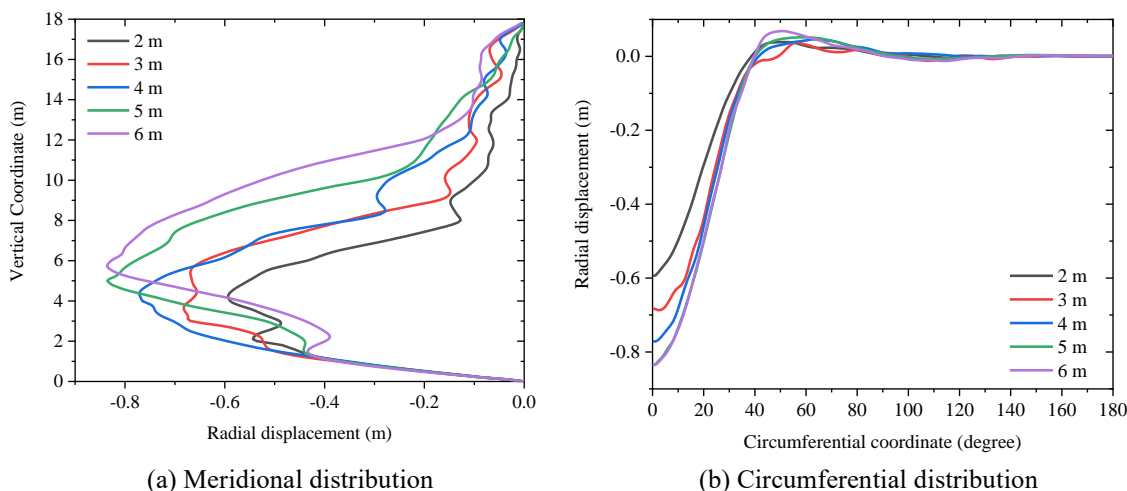

(a) Meridional distribution

(b) Circumferential distribution

Fig. 17. Radial displacement distributions along the meridian $\theta = 0°$ (a) and the circumference with largest radial displacement (b) at $t = 100$ ms.

4.4. Effect of the dimension of the steel I-section beam

The effect of the dimensions of steel I-section beams on the dynamic response of the stiffened steel tank was investigated in this section. Dimensions of steel I-section beams are listed in Table 1. The dimensions of the steel I-section beam increased as the type number increased.

Fig. 18 shows the deformation shapes of the stiffened steel tank for various dimensions at $t = 100$ ms. Fig. 19 illustrates radial displacement distributions along the meridian $\theta = 0°$ and the circumference with the largest radial displacement at $t = 100$ ms. The deformation and maximum radial displacement decreased as the dimensions of the steel I-section beam increased. Furthermore, the maximum deformation zone moved downward as the dimensions increased.

The reason is that Larger beam dimensions, particularly increased web height, result in a higher moment of inertia. This directly increases the beam's resistance to bending, allowing it to better withstand the out-of-plane forces from the blast shock wave. Besides, larger web areas increase the shear capacity of the beams. This is crucial for resisting the high shear forces that can develop near the connections between the beams and the tank wall during blast loading. Moreover, Larger beam dimensions typically mean a larger contact area between the beam and the tank wall. This helps to distribute the forces more effectively at the connection points, reducing stress concentrations that could lead to local failures. Furthermore, larger beams have more material available for plastic

deformation. This allows them to absorb more blast energy through plastic work, reducing the energy transferred to the tank wall. Consequently, the deformation and maximum radial displacement decreased as the dimensions of the steel I-section beam increased.
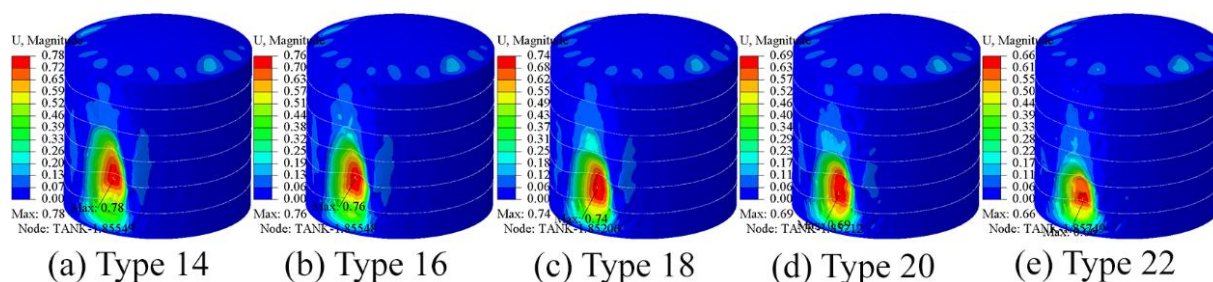

(a) Type 14   (b) Type 16   (c) Type 18   (d) Type 20   (e) Type 22

Fig. 18. Deformation shapes of the stiffened steel tank for different dimensions at t=100 ms.

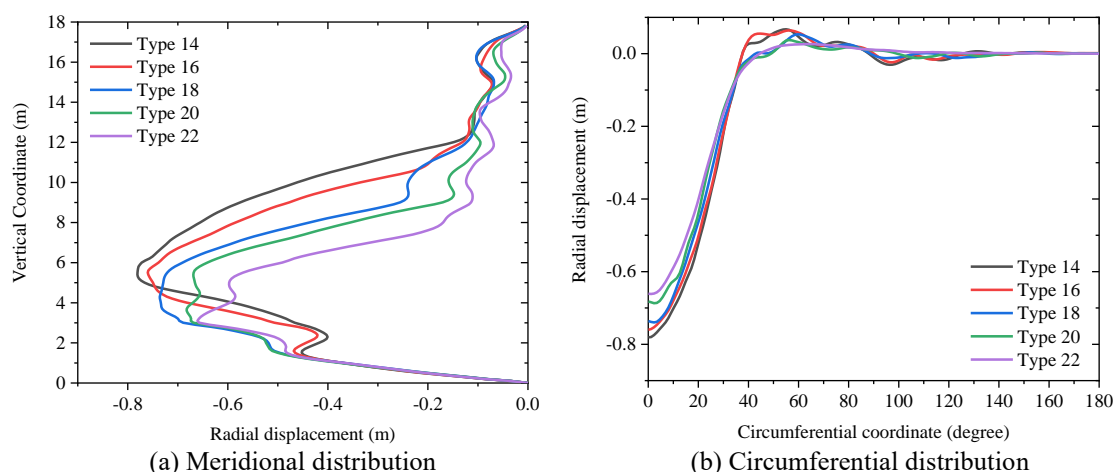(a) Meridional distribution

(b) Circumferential distribution

Fig. 19. Radial displacement distributions along the meridian $\theta = 0^\circ$ (a) and the circumference with the largest radial displacement (b) at $t = 100$ ms.

4.5. Discussion

The results presented in this study provide valuable insights into the dynamic response and blast resistance of large vertical steel storage tanks equipped with horizontal stiffening rings. The findings contribute to the understanding of how these stiffening measures can mitigate the effects of blast loading on thin-walled structures, which are particularly vulnerable to catastrophic failures in the event of an explosion.

The numerical simulations revealed that the presence of horizontal stiffening rings significantly enhances the overall stability and stiffness of the steel tank. The stiffening rings act as barriers, impeding the direct transmission of blast energy onto the cylindrical shell and reducing the amount of energy absorbed by the shell through deformation. Besides, the beams redistributed stresses, and provided increased bending and hoop stress resistance. Consequently, the deformation of the stiffened tank is less severe compared to an unstiffened configuration.

The study also investigated the effects of varying the vertical spacing between adjacent stiffening rings and the dimensions of the stiffening rings themselves. Increasing the vertical spacing or decreasing the dimensions of the stiffening rings led to more significant deformation and maximum radial displacement of the tank. These findings highlight the need for optimizing the design parameters of the stiffening ring system to achieve the desired level of blast resistance while considering practical and economic constraints. By comparing Figs. 16, 17 with Figs. 18, 19, it can be seen that reducing vertical spacing between adjacent stiffening rings is more beneficial for enhancing the blast resistance performance of the storage tank than increasing dimensions of the stiffening rings. The method of reducing the vertical spacing should be prioritized to enhance the anti-explosion performance for blast resistance design. Therefore, in this paper, a vertical spacing of 2 m for the stiffening rings is optimal. Moreover, since the blast resistance performance of the storage tank increases with the dimension of the stiffening rings In a word, a type 22 stiffening ring with the vertical spacing of 2 m represent the best for blast resistance design of a 5000 m³

fixed-roof storage tank.

The results obtained from this research have practical implications for the structural optimization and anti-blast design of large vertical steel storage tanks. By incorporating appropriately spaced and dimensioned horizontal stiffening rings, the blast resistance capabilities of these thin-walled structures can be significantly enhanced, mitigating the risk of catastrophic failures and potential hazardous material releases in the event of an explosion. Furthermore, as oil tank farms generally include multiple storage tanks, enhancing the blast resistance of the tanks through stiffening rings can reduce or prevent the risk of adjacent tank failures caused by explosion accidents, thus preventing the further escalation of the incident and avoiding ultimately catastrophic accidents.

However, the storage tank adopted in this paper was an empty tank without any liquid medium inside. Therefore, the effects of sloshing and energy absorption of the liquid medium on the dynamic response of the storage tank under blast loading are not taken into account. It is necessary to conduct further research in future studies. Additionally, while the current study investigated the effects of horizontal stiffening rings, future work could explore the potential benefits of incorporating other anti-blast measures, such as reinforced concrete bunds, or explosion-protection walls, in conjunction with the stiffening ring system. Such a holistic approach could further enhance the blast resistance capabilities of large vertical steel storage tanks and contribute to the development of comprehensive safety guidelines and design standards. Besides, the effects of explosive mass and unevenly spaced horizontal stiffening rings on the dynamic response of the storage tank under blast loading are also worth further investigation.

5. Conclusions

This study aimed to investigate the dynamic response behaviors and reliability enhancement of stiffened steel tanks under blast loading. The research focused on comparing stiffened and unstiffened tanks, and analyzing the effects of vertical spacing and dimensions of steel I-section beams on the tank's reliability under explosive conditions. The following conclusions can be drawn.

(1) The deformation shapes of the stiffened steel tank were weaker, and the radial displacements were smaller compared to an unstiffened steel tank, indicating improved blast resistance due to the steel I-section beams.

(2) The addition of horizontal steel I-section beams enhanced the overall stiffness and stability of the steel tank under blast loading. The beams redistributed stresses, and provided increased bending and hoop stress resistance, mitigating excessive deformations and improving blast resistance of the steel tank.

(3) The dimensions of the steel I-section beams, including web height and flange width, also affected the blast resistance of the stiffened steel tank. Larger beam dimensions contribute to increased bending and shear stiffness, resulting in smaller deformations and better blast resistance of the steel tank.

References

1. Zhao J, Zhang X, Zhang J, et al. Experimental study on the flame length and burning behaviors of pool fires with different ullage heights. *Energy* 2022; 246: 123397. https://doi.org/10.1016/j.energy.2022.123397.

2. Yang Y, Chen G and Reniers G. Vulnerability assessment of atmospheric storage tanks to floods based on logistic regression. *Reliability Engineering & System Safety* 2020; 196: 106721. https://doi.org/10.1016/j.ress.2019.106721.

3. Cai Y, Jiang X, Wang S, et al. Experimental study on explosion overpressure and flame propagation characteristics of simulated vertical dome oil tank. *Journal of Loss Prevention in the Process Industries* 2022; 76: 104752. https://doi.org/10.1016/j.jlp.2022.104752.

4. Megdiche I, Atherton W, Allanson D, et al. Effect of mitigation on the catastrophic failure of storage tanks. *Journal of Loss Prevention in the Process Industries* 2022; 80: 104852. https://doi.org/10.1016/j.jlp.2022.104852.

5. Yang J, Zhang B, Chen L, et al. Improved solid radiation model for thermal response in large crude oil tanks. *Energy* 2023; 284: 128572. https://doi.org/10.1016/j.energy.2023.128572.

6. Meng Z, Ma C and Xie Y. Influence of impact load form on dynamic response of chock-shield support. *Eksploatacja i Niezawodność – Maintenance and Reliability* 2023; 25. 10.17531/ein/168316.

7. Duong DH, Hanus JL, Bouazaoui L, et al. Response of a tank under blast loading -- part I: experimental characterisation of blast loading arising from a gas explosion. *European Journal of Environmental and Civil Engineering* 2012; 16: 1023-1041. 10.1080/19648189.2012.699741.

8. Clubley SK. Non-linear long duration blast loading of cylindrical shell structures. *Engineering Structures* 2014; 59: 113-126. 10.1016/j.engstruct.2013.10.030.

9. Clubley SK. Long duration blast loading of cylindrical shell structures with variable fill level. *Thin-Walled Structures* 2014; 85: 234-249. https://doi.org/10.1016/j.tws.2014.08.021.

10. Zhang Q, Zhou G, Hu Y, et al. Risk evaluation and analysis of a gas tank explosion based on a vapor cloud explosion model: A case study. *Engineering Failure Analysis* 2019; 101: 22-35. https://doi.org/10.1016/j.engfailanal.2019.03.003.

11. Wang Y and Zhou H. Numerical study of water tank under blast loading. *Thin-Walled Structures* 2015; 90: 42-48. https://doi.org/10.1016/j.tws.2015.01.012.

12. Zhang BY, Li HH and Wang W. Numerical study of dynamic response and failure analysis of spherical storage tanks under external blast loading. *Journal of Loss Prevention in the Process Industries* 2015; 34: 209-217. 10.1016/j.jlp.2015.02.008.

13. Hu K and Zhao Y. Numerical simulation of internal gaseous explosion loading in large-scale cylindrical tanks with fixed roof. *Thin-Walled Structures* 2016; 105: 16-28. http://dx.doi.org/10.1016/j.tws.2016.03.026.

14. Pickerd V, Bornstein H, McCarthy P, et al. Analysis of the structural response and failure of containers subjected to internal blast loading. *International Journal of Impact Engineering* 2016; 95: 40-53. https://doi.org/10.1016/j.ijimpeng.2016.04.010.

15. Abo-Elkhier M and Muhammad K. Failure analysis of an exploded large-capacity liquid storage tank using finite element analysis. *Engineering Failure Analysis* 2020; 110: 104401. https://doi.org/10.1016/j.engfailanal.2020.104401.

16. Hu K, Chen G, Zhou C, et al. Dynamic response of a large vertical tank impacted by blast fragments from chemical equipment. *Safety Science* 2020; 130: 104863. https://doi.org/10.1016/j.ssci.2020.104863.

17. Li J and Hao H. Numerical simulation of medium to large scale BLEVE and the prediction of BLEVE's blast wave in obstructed environment. *Process Safety and Environmental Protection* 2021; 145: 94-109. https://doi.org/10.1016/j.psep.2020.07.038.

18. Li J and Hao H. Numerical and analytical prediction of pressure and impulse from vented gas explosion in large cylindrical tanks. *Process Safety and Environmental Protection* 2019; 127: 226-244. https://doi.org/10.1016/j.psep.2019.05.019.

19. Chen G, Wang F, Zhou C, et al. Dynamic Response Analysis of Large Arch-Roof Oil Tank Subjected to the Coupling Impact of Two-Source Blast Waves Based on Finite Element Method. *Journal of Failure Analysis and Prevention* 2020; 20: 333-347. https://doi.org/10.1007/s11668-020-00833-w.

20. Rokhy H and Mostofi TM. 3D numerical simulation of the gas detonation forming of aluminum tubes considering fluid-structure interaction and chemical kinetic model. *Thin-Walled Structures* 2021; 161: 107469. https://doi.org/10.1016/j.tws.2021.107469.

21. Studziński R, Sumelka W, Malendowski M, et al. Sandwich panel subjected to blast wave impact and accelerated fragments. *Eksploatacja i Niezawodność – Maintenance and Reliability* 2024; 26. 10.17531/ein/183698.

22. Jiang H, Ding L, Ji J, et al. Building reliability of risk assessment of domino effects in chemical tank farm through an improved uncertainty analysis method. *Reliability Engineering & System Safety* 2024; 252: 110388. https://doi.org/10.1016/j.ress.2024.110388.

23. Su QQ and Zhai XM. Dynamic response of single-layer reticulated shell with explosion-protection wall under blast loading. *Thin-Walled Structures* 2018; 127: 389-401. 10.1016/j.tws.2017.12.008.

24. Zheng C, Kong X-s, Wu W-g, et al. Experimental and numerical studies on the dynamic response of steel plates subjected to confined blast loading. *International Journal of Impact Engineering* 2018; 113: 144-160. https://doi.org/10.1016/j.ijimpeng.2017.11.013.

25. Bornstein H, Ryan S and Mouritz AP. Evaluation of blast protection using novel-shaped water-filled containers: Experiments and

simulations. *International Journal of Impact Engineering* 2019; 127: 41-61. https://doi.org/10.1016/j.ijimpeng.2019.01.006.

26. Jiang Y, Zhang B, Wei J, et al. Study on the dynamic response of polyurea coated steel tank subjected to blast loadings. *Journal of Loss Prevention in the Process Industries* 2020; 67: 104234. https://doi.org/10.1016/j.jlp.2020.104234.

27. Wu T, Jiang N, Zhou C, et al. Evaluate of anti-explosion for high-pressure gas steel pipeline subjected to ground explosion. *Journal of Constructional Steel Research* 2020: 106429. https://doi.org/10.1016/j.jcsr.2020.106429.

28. Jiang Y, Zhang B, Wang L, et al. Dynamic response of polyurea coated thin steel storage tank to long duration blast loadings. *Thin-Walled Structures* 2021; 163: 107747. https://doi.org/10.1016/j.tws.2021.107747.

29. Gan L, Zong Z, Gao C, et al. Influence of shape of cuboid explosives on response of plates subjected to blast loads. *Thin-Walled Structures* 2022; 174: 109077. https://doi.org/10.1016/j.tws.2022.109077.

30. Wang Z, Hu K and Zhao Y. Doom-roof steel tanks under external explosion: Dynamic responses and anti-explosion measures. *Journal of Constructional Steel Research* 2022; 190: 107118. https://doi.org/10.1016/j.jcsr.2021.107118.

31. Zhao S, Huo J, Xu R, et al. Prevention of bund overtopping after a catastrophic tank failure accident: Effects of bund design, liquids and scale-up. *Process Safety and Environmental Protection* 2022; 166: 41-56. https://doi.org/10.1016/j.psep.2022.07.062.

32. GB50341-2014: Code for design of vertical cylindrical welded steel oil tanks. 2015.

33. API 650: Weld steel tanks for oil storage. American Petroleum Institute Washington, DC, 2007.

34. Liu Y, Du Y, Zhang Z, et al. Dynamic response and vibration modes of multi-layer wound cylindrical shell for hydrogen storage under external blast loading. *International Journal of Hydrogen Energy* 2024; 54: 1242-1250. https://doi.org/10.1016/j.ijhydene.2023.10.085.

35. Upadhyay AK, Ramdas C and Simha K. Response of cylindrical tube under blast: experiment and numerical simulation. *International Journal of Materials and Structural Integrity* 2018; 12: 339-352. https://doi.org/10.1504/IJMSI.2018.095893.

36. Ullah A, Ahmad F, Jang H-W, et al. Review of analytical and empirical estimations for incident blast pressure. *KSCE Journal of Civil Engineering* 2017; 21: 2211-2225. 10.1007/s12205-016-1386-4.

37. Jeremić R and Bajić Z. An approach to determining the TNT equivalent of high explosives. *Scientific-Technical Review* 2006; 56: 58-62. https://doi.org/10.13140/RG.2.1.2316.3363.